B0834+06 - A trip down Scintillation Lane

Observations of some further Pulsed Radio Sources

by
J. D. H. PILKINGTON
A. HEWISH
S. J. BELL
T. W. COLE

Mullard Radio Astronomy Observatory,
Cavendish Laboratory,
University of Cambridge

Details are now given of three of the four pulsating radio sources discovered at Cambridge.

IN a recent communication[1] an account was given of the discovery of a new class of radio source characterized by the emission of short pulses of radiation having an extremely constant repetition frequency. The records on which the source was first detected were taken during a survey for the investigation of compact radio sources using the method of interplanetary scintillation. Following the recognition of the first pulsed source the survey records, which covered the region $-08° < \delta < 44°$, were examined for evidence of further similar sources. Where these records indicated that the intensity fluctuations of a particular source were more impulsive than those caused by interplanetary scintillation, further observations were made. These led to the discovery of three additional pulsed sources. Even though each area of sky was observed on about twenty separate occasions during this survey,
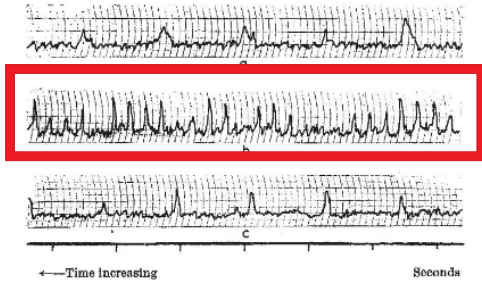

Fig. 1. Pulses observed with a recording time constant of about 0·03 s on March 21, 1968. (a) CP.0834. (b) CP.0950, during a period of intense activity. (c) CP.1133.

←—Time increasing   Seconds
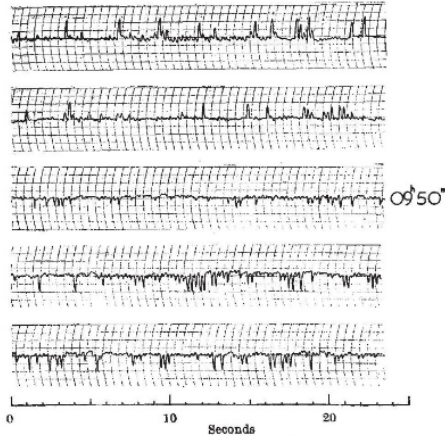

Fig. 2. A continuous set of observations of CP.0950 at a time of strong activity, showing the irregular variations of intensity from pulse to pulse. The deflexions change sign as the source moves through the interference pattern of the aerial. Recording time constant 0·1 s.

the large day-to-day variations of flux density from the known sources indicate that this programme should not be regarded as an exhaustive search of the entire region, and observations are continuing.

The three sources and the original one have been given numbers of the form CP.1919 to indicate the Cambridge pulsed source at $\alpha = 19^h\ 19^m$.

Observations of some further Pulsed Radio Sources

by
J. D. H. PILKINGTON
A. HEWISH
S. J. BELL
T. W. COLE
Mullard Radio Astronomy Observatory,
Cavendish Laboratory,
University of Cambridge

Details are now given of three of the four pulsating radio sources discovered at Cambridge.

IN a recent communication[1] an account was given of the discovery of a new class of radio source characterized by the emission of short pulses of radiation having an extremely constant repetition frequency. The records on which the source was first detected were taken during a survey for the investigation of compact radio sources using the method of interplanetary scintillation. Following the recognition of the first pulsed source the survey records, which covered the region $-08° < \delta < 44°$, were examined for evidence of further similar sources. Where those records indicated that the intensity fluctuations of a particular source were more impulsive than those caused by interplanetary scintillation, further observations were made. These led to the discovery of three additional pulsed sources. Even though each area of sky was observed on about twenty separate occasions during this survey,
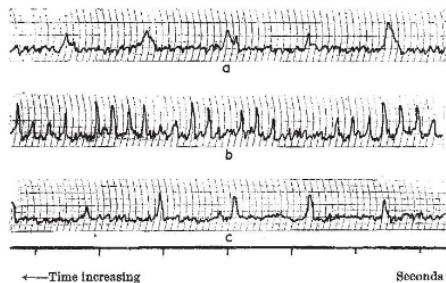

Fig. 1. Pulses observed with a recording time constant of about 0·03 s on March 21, 1968. (a) CP.0834. (b) CP.0950, during a period of intense activity. (c) CP.1133.
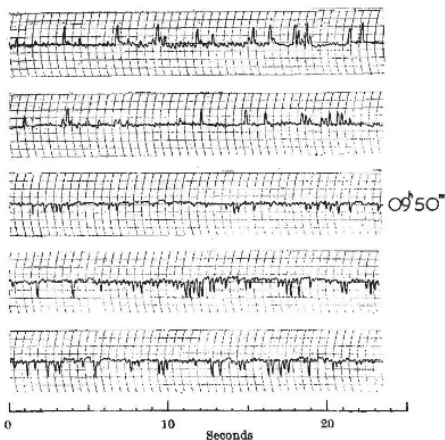
←—Time Increasing   Seconds

Fig. 2. A continuous set of observations of CP.0950 at a time of strong activity, showing the irregular variations of intensity from pulse to pulse. The deflexions change sign as the source moves through the interference pattern of the aerial. Recording time constant 0·1 s.

the large day-to-day variations of flux density from the known sources indicate that this programme should not be regarded as an exhaustive search of the entire region, and observations are continuing.

The three sources and the original one have been given numbers of the form CP.1919 to indicate the Cambridge pulsed source at $\alpha = 19^h\ 19^m$.

Table 1. CHARACTERI

	CP.0834
$\alpha(1950\cdot0)$	$08^h\ 34^m\ 07^s \pm 15^s$
$\delta(1950\cdot0)$	$07° 00' \pm 45'$
P_0 (s)	$1\cdot27379 \pm 0\cdot00008$
$-\left(\dfrac{d\nu}{dt}\right)$ at 81·5 MHz (MHz s^{-1})	$5\cdot3 \pm 0\cdot5$
Integrated electron density Nl (cm^{-3} pc)	12 ± 1
Emitted pulse duration (Gaussian) (ms)	35 ± 10
Mean flux density at 81·5 MHz (10^{-26} W m^{-2} Hz^{-1})	$0\cdot3$
l^{II}	$220°$
b^{II}	$26°$

Observations of some further Pulsed Radio Sources

by
J. D. H. PILKINGTON
A. HEWISH
S. J. BELL
T. W. COLE
Mullard Radio Astronomy Observatory,
Cavendish Laboratory,
University of Cambridge

Details are now given of three of the four pulsating radio sources discovered at Cambridge.

IN a recent communication[1] an account was given of the discovery of a new class of radio source characterized by the emission of short pulses of radiation having an extremely constant repetition frequency. The records on which the source was first detected were taken during a survey for the investigation of compact radio sources using the method of interplanetary scintillation. Following the recognition of the first pulsed source the survey records, which covered the region $-08° < \delta < 44°$, were examined for evidence of further similar sources. Where these records indicated that the intensity fluctuations of a particular source were more impulsive than those caused by interplanetary scintillation, further observations were made. These led to the discovery of three additional pulsed sources. Even though each area of sky was observed on about twenty separate occasions during this survey,
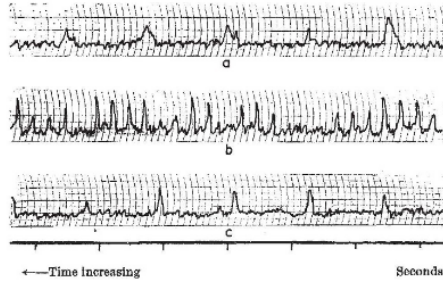

Fig. 1. Pulses observed with a recording time constant of about 0·03 s on March 21, 1968. (a) CP.0834. (b) CP.0950, during a period of intense activity. (c) CP.1133.
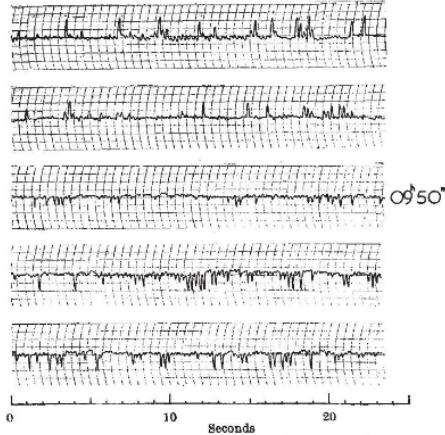

Fig. 2. A continuous set of observations of CP.0950 at a time of strong activity, showing the irregular variations of intensity from pulse to pulse. The deflexions change sign as the source moves through the interference pattern of the aerial. Recording time constant 0·1 s.

the large day-to-day variations of flux density from the known sources indicate that this programme should not be regarded as an exhaustive search of the entire region and observations are continuing.

The three sources and the original one have been given numbers of the form CP.1919 to indicate the Cambridge pulsed source at $\alpha = 19^h 19^m$.
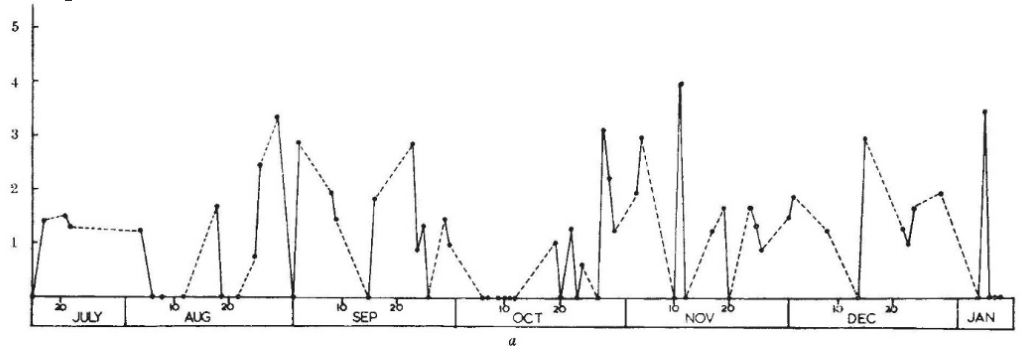
Table 1. CHARACTERI...

	CP.0834
$\alpha(1950\cdot0)$	$08^h 34^m 07^s \pm 15^s$
$\delta(1950\cdot0)$	$07° 00' \pm 45'$
P_0 (s)	$1\cdot27379 \pm 0\cdot00008$
$-\left(\dfrac{d\nu}{dt}\right)$ at 81·5 MHz (MHz s^{-1})	$5\cdot3 \pm 0\cdot5$
Integrated electron density Nl (cm^{-3} pc)	12 ± 1
Emitted pulse duration (Gaussian) (ms)	35 ± 10
Mean flux density at 81·5 MHz (10^{-26} W m^{-2} Hz^{-1})	$0\cdot3$
l^{II}	$220°$
b^{II}	$26°$

Scintillating!

Interstellar fringes from pulsar B0834+06

Barney J. Rickett,[1] Andrew G. Lyne[2] and Yashwant Gupta[3]

[1] *Department of Electrical and Computer Engineering, University of California, San Diego, CA 92093-0407, USA*
[2] *University of Manchester, Nuffield Radio Astronomy Laboratories, Jodrell Bank, Macclesfield SK11 9DL*
[3] *National Centre for Radio Astrophysics, TIFR, Post Bag 3, Ganeshkhind, Pune 411 007, India*

ABSTRACT

Observations at Jodrell Bank are reported of very fine modulations of the dynamic spectra of interstellar scintillation (ISS) from pulsar PSR B0834+06. These fringes have a period in radio frequency of 45 kHz, which is about 100 times smaller than the largest bandwidth due to normal ISS of the pulsar at the central observing frequency of 408 MHz. Analysis shows good consistency with a model in which two ray-bundles intersect and interfere creating the fringes, from which a 22-μs delay difference is inferred. The separation between the bundles is greater than 4 mas which is more than 10 times their angular diameter. Such a large ratio cannot be due to an inner scale that cuts off the pervasive turbulent density spectrum responsible for the diffractive angular broadening.
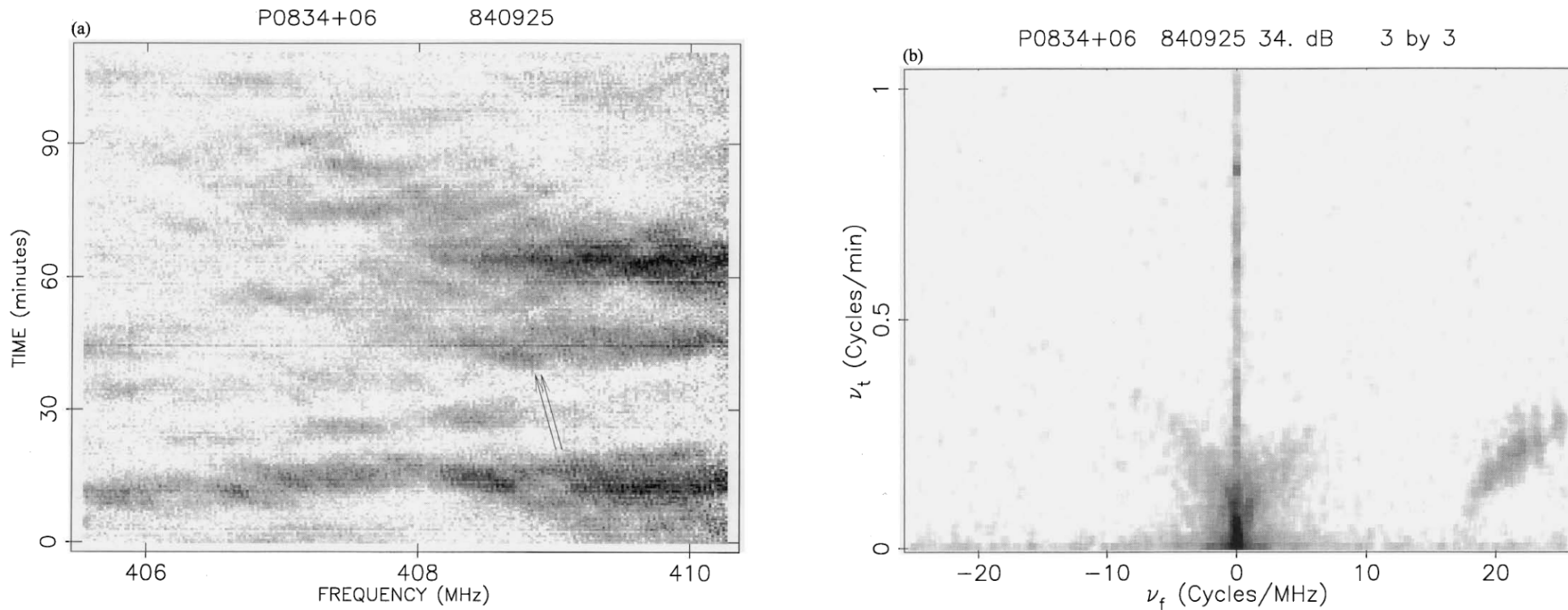
The fringing was observed on four occasions over 30 d and so is similar to the 'extreme scattering events' observed in other sources. 3 au is the scale inferred, and various possible structures in the interstellar plasma density are considered. A stochastic refraction model is proposed, in which many isolated regions in a layer of parsec thickness randomly build up enhanced angles of refraction. Normally neighbouring ray-paths do not intersect. However, occasionally their angles are large enough to cause interference and the associated fringes. A specific model is proposed in which the ionized refracting layer surrounds a warm H I cloud, with anisotropic density irregularities of 0.25 electron cm^{-3}, which could be in equilibrium with the normal interstellar pressure.

Key words: plasmas – scattering – turbulence – pulsars: individual: PSR B0834+06 – ISM: general.
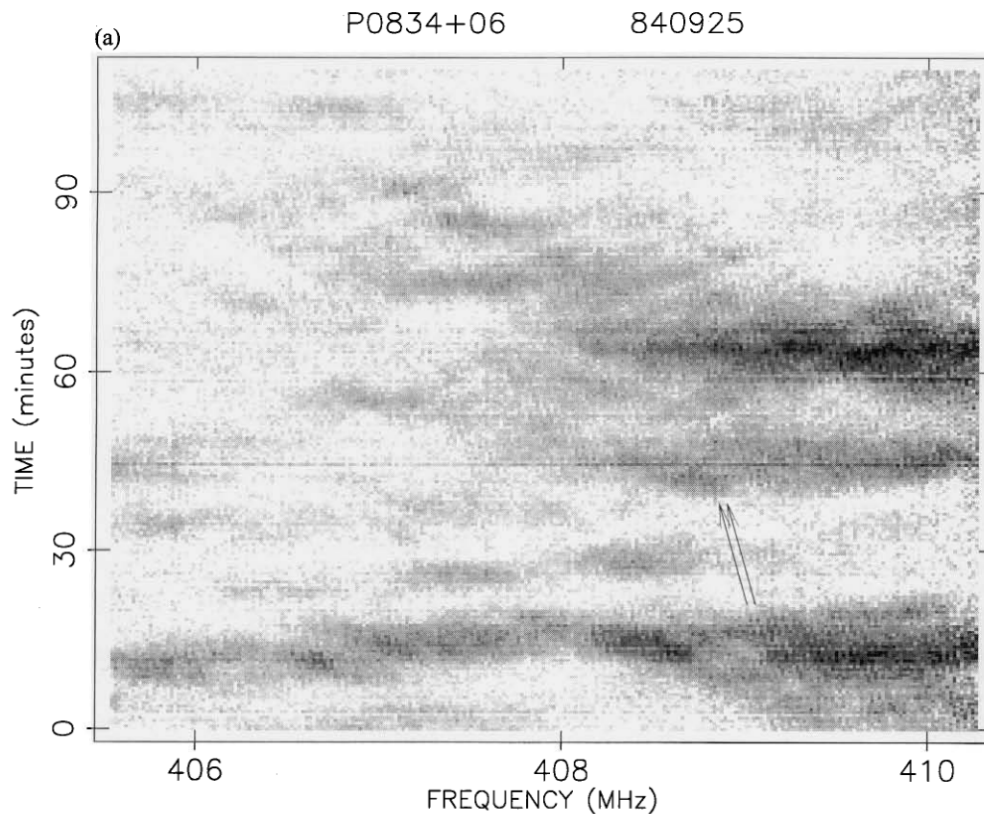

Figure 1. (a) Dynamic spectrum of PSR B0834+06 on 1984 September 25. Pulse flux averaged over 29 s and 19.5 kHz is plotted as a grey-scale with dot density linearly proportional to flux density, ranging from white at 6 per cent of the peak flux to black at 75 per cent of the peak flux; values outside these limits saturate the display. The fine modulations (fringes with 45-kHz period) can best be seen by tipping the page away and looking along the arrowed direction.

$$I(t, f) \xrightarrow[\text{Power Spectrum}]{\text{2D FFT, squared}} |\tilde{I}(f_t, f_\nu)|^2$$

(a)

P0834+06   840925

TIME (minutes)

FREQUENCY (MHz)

(b)

P0834+06   840925 34. dB   3 by 3

ν_t (Cycles/min)

ν_f (Cycles/MHz)

Figure 1. (a) Dynamic spectrum of PSR B0834+06 on 1984 September 25. Pulse flux averaged over 29 s and 19.5 kHz is plotted as a grey-scale with dot density linearly proportional to flux density, ranging from white at 6 per cent of the peak flux to black at 75 per cent of the peak flux; values outside these limits saturate the display. The fine modulations (fringes with 45-kHz period) can best be seen by tipping the page away and looking along the arrowed direction.

$$|\tilde{I}(f_t, f_\nu)|^2$$

STINEBRING ET AL.

Stinebring et al. 2001
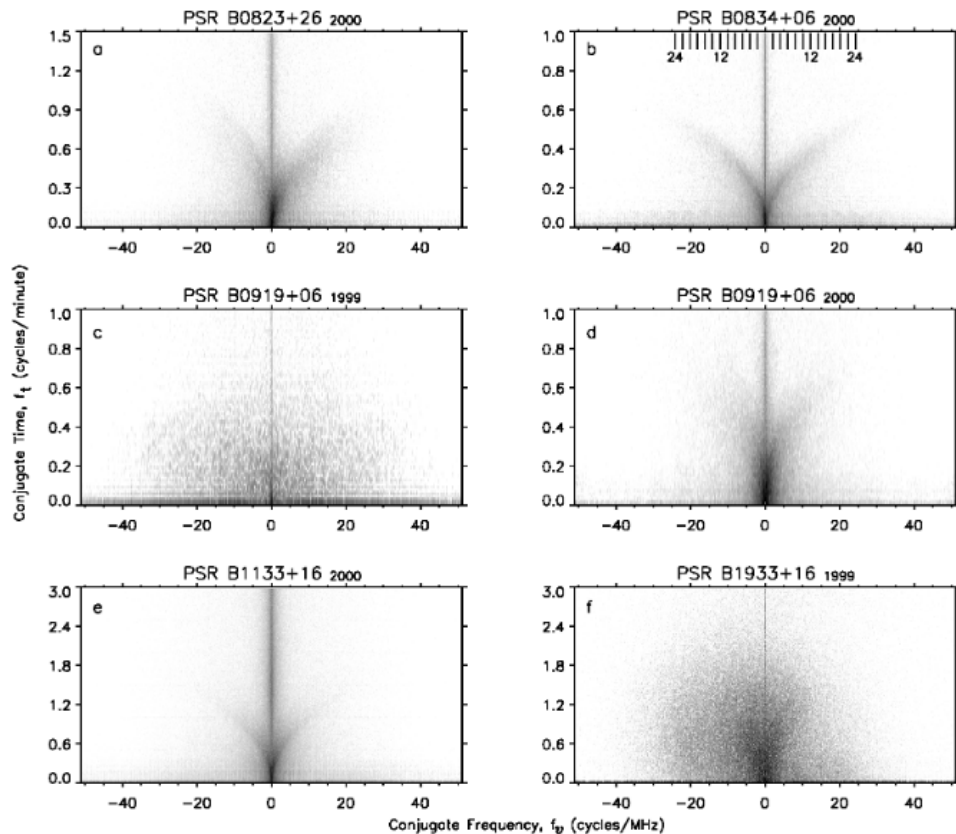
"Palm Frond" structure surprisingly common

What causes this?

$$|\tilde{I}(f_t, f_\nu)|^2$$

PSR B0834+06 2000

f_t

f_ν
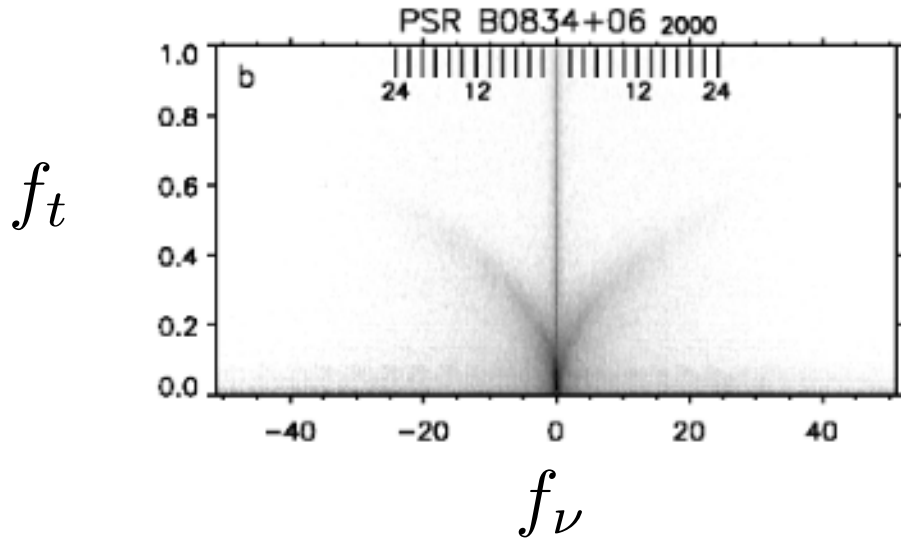
"Palm Frond" structure surprisingly common

What causes this?

Try swapping axes...

$$|\tilde{I}(f_t, f_\nu)|^2$$

f_t

f_ν
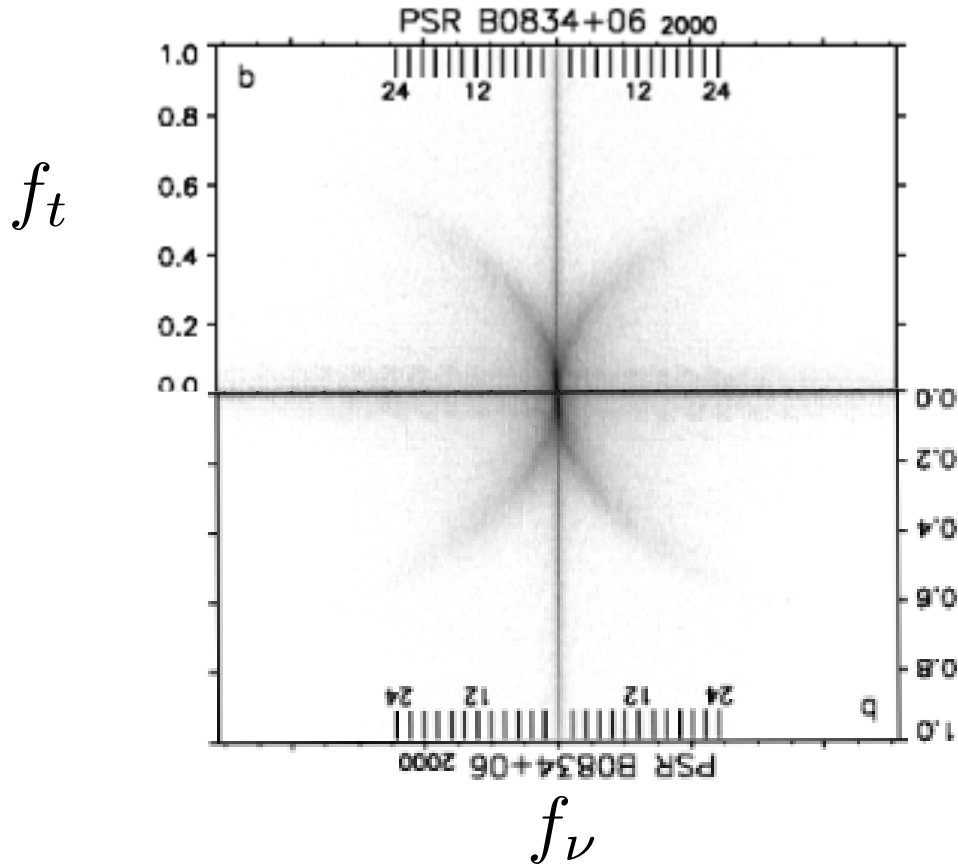
"Palm Frond" structure surprisingly common

What causes this?

Try swapping axes…

FT of real function, so point symmetric
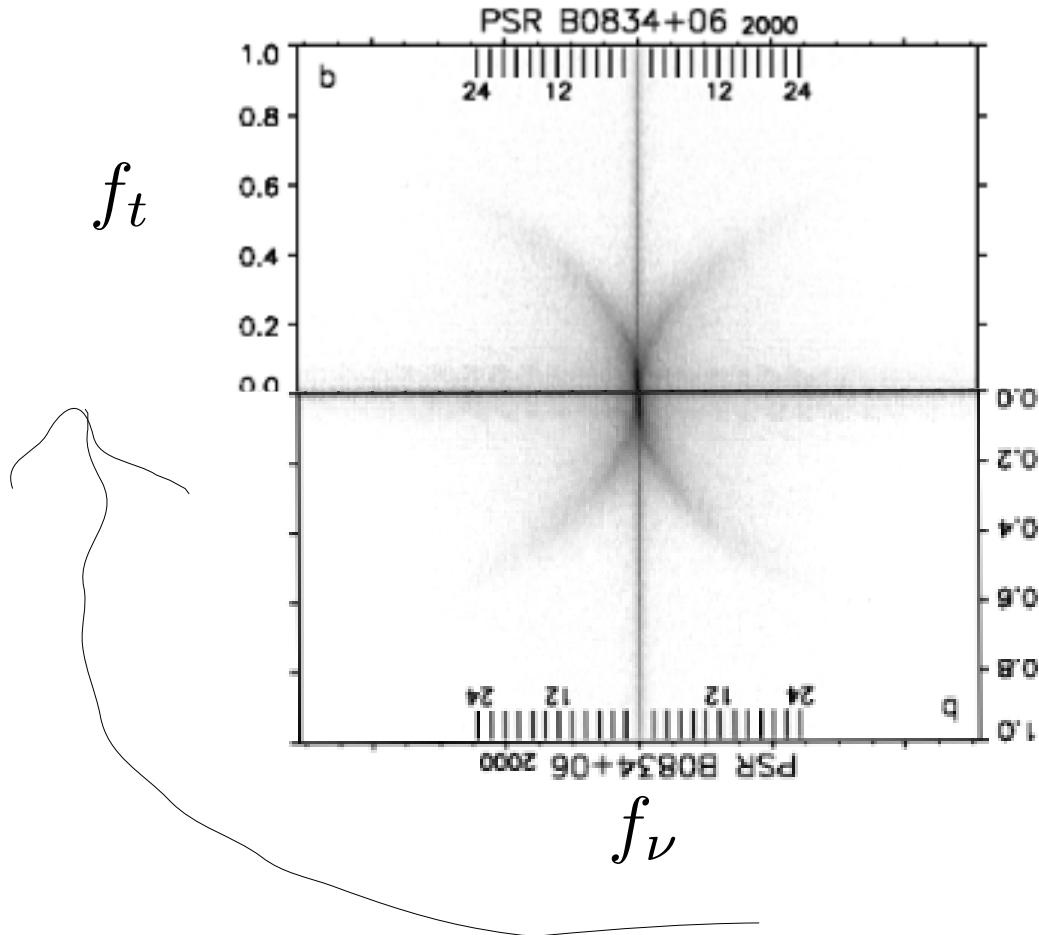
$$|\tilde{I}(f_t, f_\nu)|^2$$

PSR B0834+06 2000

f_t

f_ν

"Palm Frond" structure surprisingly common

What causes this?

Try swapping axes…

FFT of real function, so point symmetric

$$|\tilde{I}(f_t, f_\nu)|^2$$

f_t

f_ν

"Palm Frond" structure surprisingly common

What causes this?

Try swapping axes…

FFT of real function, so point symmetric

$$|\tilde{I}(f_t, f_\nu)|^2$$

f_ν

f_t

"Palm Frond" structure surprisingly common

What causes this?

Try swapping axes…

FFT of real function, so point symmetric

$$|\tilde{I}(f_t, f_\nu)|^2$$

"Palm Frond" structure surprisingly common
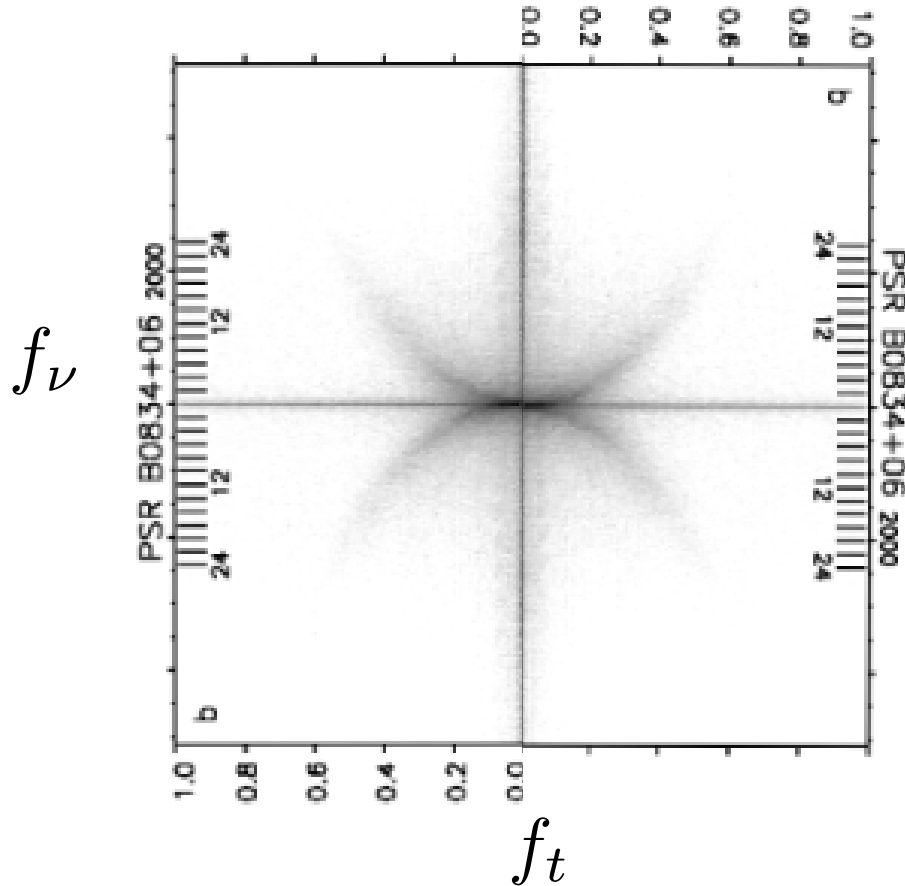
What causes this?

Try swapping axes…

FFT of real function, so point symmetric

"Palm Fronds" are Parabolae!

What causes scattered power to follow parabolae?

Interpretation of parabolic arcs in pulsar secondary spectra

M. A. Walker,[1][*] D. B. Melrose,[1] D. R. Stinebring[2] and C. M. Zhang[1]

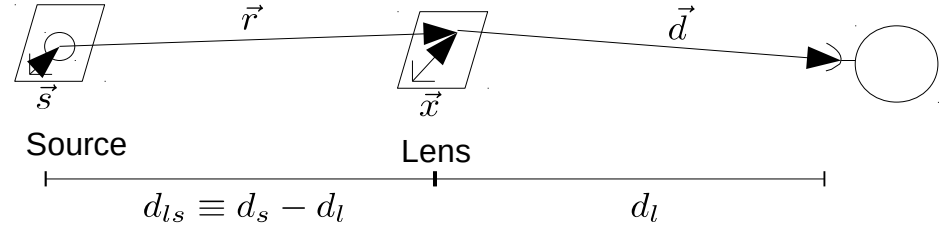[1]*School of Physics, University of Sydney, NSW 2006, Australia*
[2]*Oberlin College, Department of Physics and Astronomy, Oberlin, OH 44074, USA*

ABSTRACT
Pulsar dynamic spectra sometimes show organized interference patterns: these patterns have been shown to have power spectra that often take the form of parabolic arcs, or sequences of inverted parabolic arclets whose apexes themselves follow a parabolic locus. Here, we consider the interpretation of these arc and arclet features. We give a statistical formulation for the appearance of the power spectra, based on the stationary phase approximation to the Fresnel–Kirchoff integral. We present a simple analytic result for the power spectrum expected in the case of highly elongated images and a single-integral analytic formulation appropriate to the case of axisymmetric images. Our results are illustrated in both the ensemble-average and snapshot regimes. Highly anisotropic scattering appears to be an important ingredient in the formation of the observed arclets.

Key words: pulsars: general – ISM: general.

$$E_{obs} = \int_{lens} d\vec{x}\, e^{i\phi(\vec{x})} \int_{source} d\vec{s}\, e^{i(k/d_{ls})\vec{s}\cdot\vec{x}} E(\vec{s})$$

Interpretation of parabolic arcs in pulsar secondary spectra

M. A. Walker,[1]★ D. B. Melrose,[1] D. R. Stinebring[2] and C. M. Zhang[1]

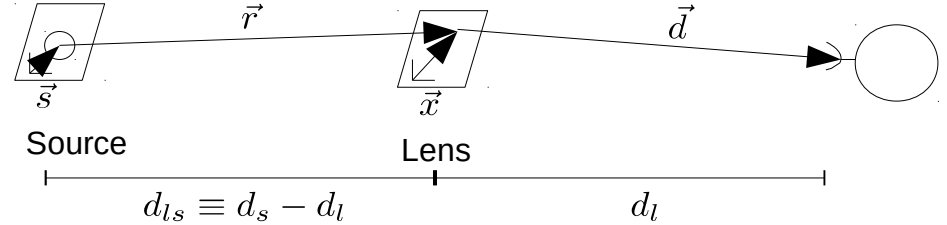[1] School of Physics, University of Sydney, NSW 2006, Australia
[2] Oberlin College, Department of Physics and Astronomy, Oberlin, OH 44074, USA

ABSTRACT
Pulsar dynamic spectra sometimes show organized interference patterns: these patterns have
been shown to have power spectra that often take the form of parabolic arcs, or sequences
of inverted parabolic arclets whose apexes themselves follow a parabolic locus. Here, we
consider the interpretation of these arc and arclet features. We give a statistical formulation
for the appearance of the power spectra, based on the stationary phase approximation to the
Fresnel–Kirchoff integral. We present a simple analytic result for the power spectrum expected
in the case of highly elongated images and a single-integral analytic formulation appropriate
to the case of axisymmetric images. Our results are illustrated in both the ensemble-average
and snapshot regimes. Highly anisotropic scattering appears to be an important ingredient in
the formation of the observed arclets.

Key words: pulsars: general – ISM: general.

$$E_{obs} = \int_{lens} d\vec{x}\, e^{i\phi(\vec{x})} \int_{source} d\vec{s}\, e^{i(k/d_{ls})\vec{s}\cdot\vec{x}} E(\vec{s})$$

"Stationary Phase Approximation"

- Pulsar is a point source

- Only points where the phase is constant
  contribute to integral

$$E_{obs} = \sum_j \mu_j e^{2\pi i \phi_j}$$

Interpretation of parabolic arcs in pulsar secondary spectra

M. A. Walker,[1][*] D. B. Melrose,[1] D. R. Stinebring[2] and C. M. Zhang[1]

[1]*School of Physics, University of Sydney, NSW 2006, Australia*
[2]*Oberlin College, Department of Physics and Astronomy, Oberlin, OH 44074, USA*

ABSTRACT
Pulsar dynamic spectra sometimes show organized interference patterns: these patterns have
been shown to have power spectra that often take the form of parabolic arcs, or sequences
of inverted parabolic arclets whose apexes themselves follow a parabolic locus. Here, we
consider the interpretation of these arc and arclet features. We give a statistical formulation
for the appearance of the power spectra, based on the stationary phase approximation to the
Fresnel–Kirchoff integral. We present a simple analytic result for the power spectrum expected
in the case of highly elongated images and a single-integral analytic formulation appropriate
to the case of axisymmetric images. Our results are illustrated in both the ensemble-average
and snapshot regimes. Highly anisotropic scattering appears to be an important ingredient in
the formation of the observed arclets.

Key words: pulsars: general – ISM: general.

$$E_{obs} = \int_{lens} d\vec{x}\, e^{i\phi(\vec{x})} \int_{source} d\vec{s}\, e^{i(k/d_{ls})\vec{s}\cdot\vec{x}} E(\vec{s})$$

"Stationary Phase Approximation"

- Pulsar is a point source

- Only points where the phase is constant
  contribute to integral

$$E_{obs} = \sum_j \mu_j e^{2\pi i \phi_j}$$

$$I = |E|^2 = |\sum_j \mu_j e^{i\phi_j}|^2 = \sum_{j,k} \mu_j \mu_k e^{i(\phi_j - \phi_k)}$$

$$I = |E|^2 = |\sum_j \mu_j e^{i\phi_j}|^2 = \sum_{j,k} \mu_j \mu_k e^{i(\phi_j - \phi_k)}$$
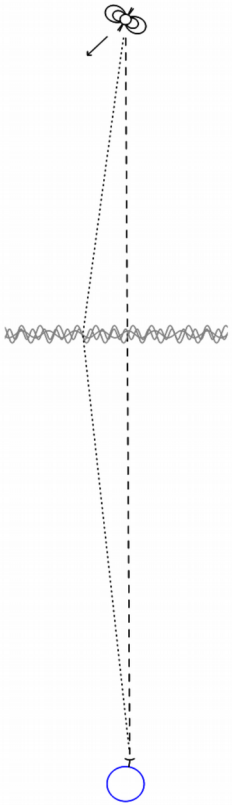
There are a discrete set of points where "Images" are formed
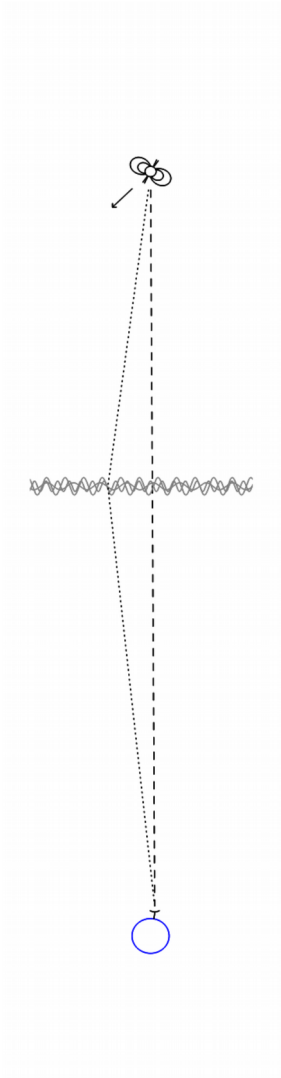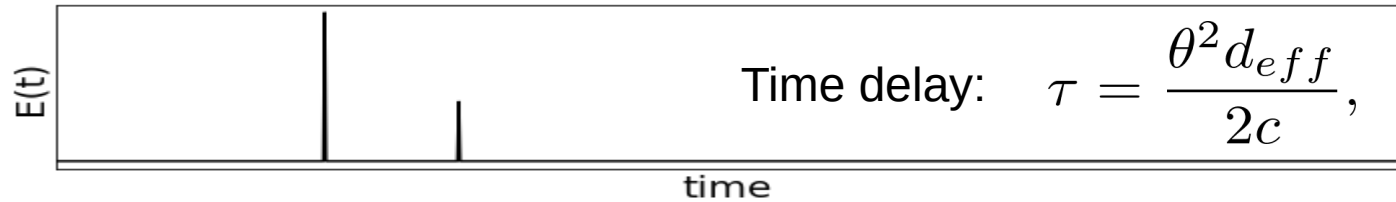
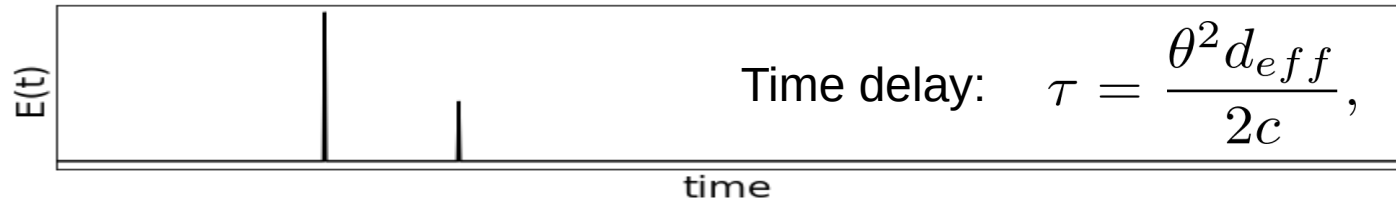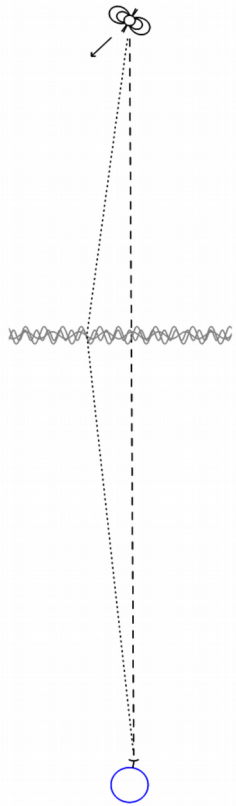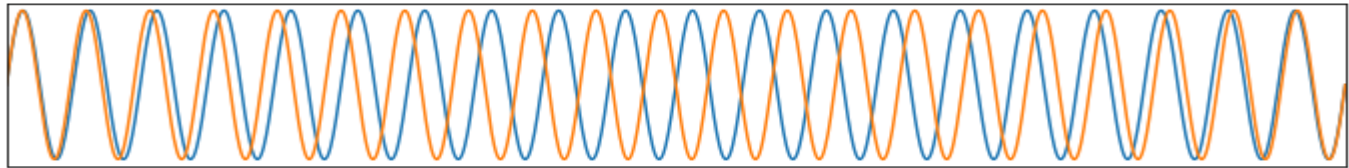We observe is the interference pattern between each pair of images

$$I = |E|^2 = |\sum_j \mu_j e^{i\phi_j}|^2 = \sum_{j,k} \mu_j \mu_k e^{i(\phi_j - \phi_k)}$$

There are a discrete set of points where "Images" are formed

We observe is the interference pattern between each pair of images

Time delay: $\tau = \dfrac{\theta^2 d_{eff}}{2c},$

E(t)

time

$$I = |E|^2 = |\sum_j \mu_j e^{i\phi_j}|^2 = \sum_{j,k} \mu_j \mu_k e^{i(\phi_j - \phi_k)}$$

There are a discrete set of points where "Images" are formed

We observe is the interference pattern between each pair of images

Time delay: $\quad \tau = \dfrac{\theta^2 d_{eff}}{2c},$

Fringe rate (or Doppler delay): $\quad f_D = \dfrac{\boldsymbol{V_{eff} \cdot \theta}}{\lambda},$

$$I = |E|^2 = |\sum_j \mu_j e^{i\phi_j}|^2 = \sum_{j,k} \mu_j \mu_k e^{i(\phi_j - \phi_k)}$$

There are a discrete set of points where "Images" are formed

We observe is the interference pattern between each pair of images

Time delay: $\tau = \dfrac{\theta^2 d_{eff}}{2c}$,
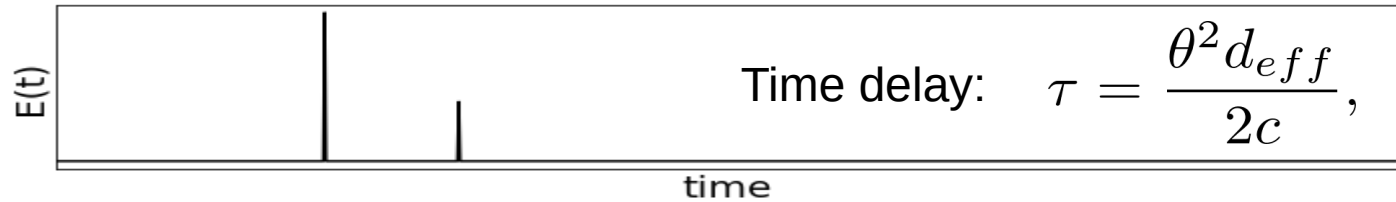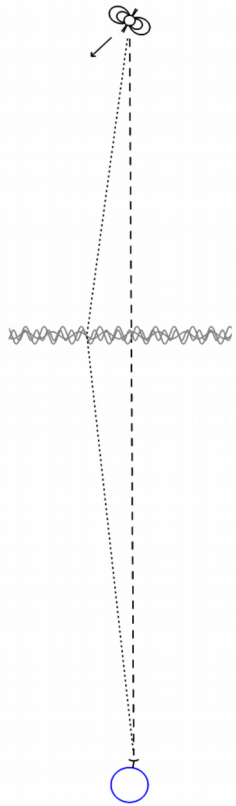
Fringe rate (or Doppler delay): $f_D = \dfrac{\boldsymbol{V_{eff} \cdot \theta}}{\lambda}$,
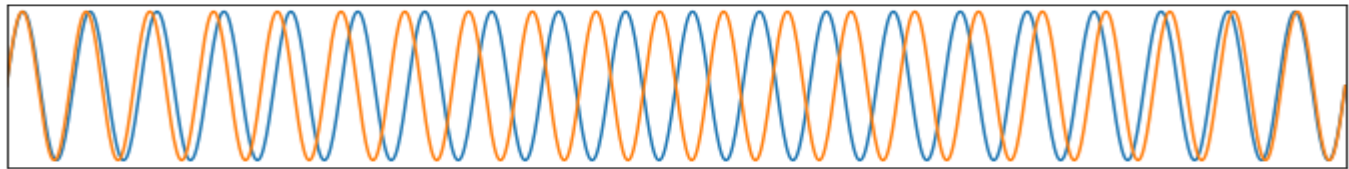
$$\tau \propto f_D^2$$

Simulated 1D Screen
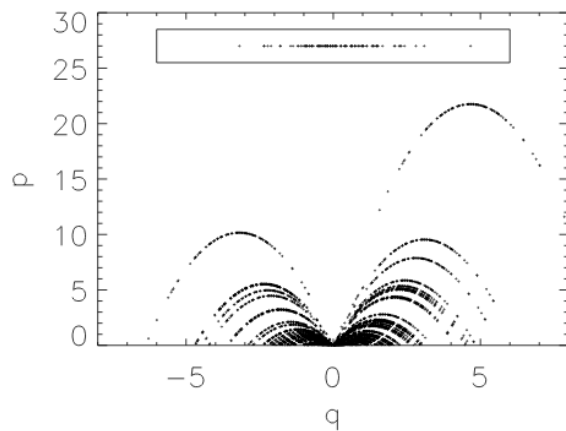
Simulated 2D Screen
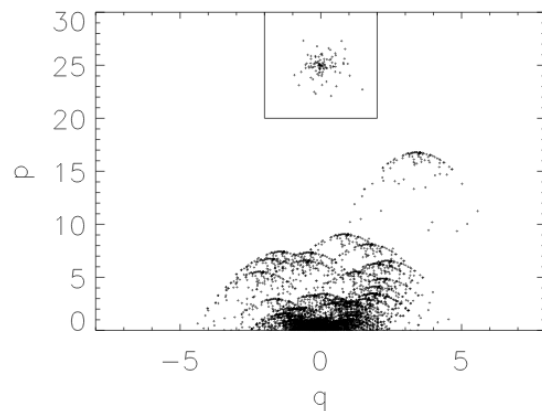
B0834+06
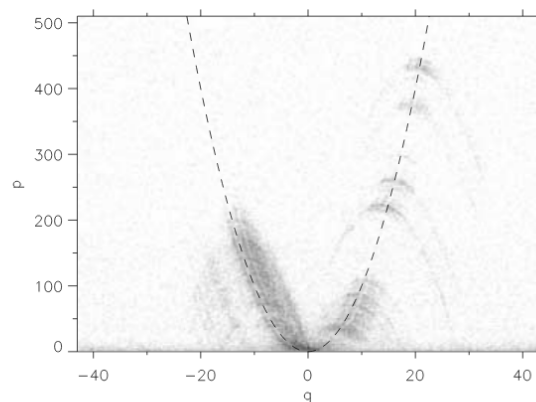
Figure 9. The secondary spectrum of PSR B0834+06 observed at 321 MHz on 2004 January 8 with the Arecibo telescope. The grey-scale is logarithmic in relative power, with white being set 3 dB above the noise floor and black being set at 5 dB below maximum power. The arclet pattern seen prominently on the right hand side of the plot persisted for more than 25 d during 2004 January and moved systematically up and to the right along the guiding parabolic arc shown by the dashed line. The axis scaling is described in the text and can be compared directly with the plots of model data. The axes in this plot are scaled in the same way as in Fig. 8, but using the values $D_p = 0.72\,\mathrm{kpc}$, $v_p = 175\,\mathrm{km\,s^{-1}}$, $\beta = 0.33$, and $\theta_o \simeq 0.72\,\mathrm{mas}$.

Interstellar holography

M. A. Walker,[1,2,3,4*] L. V. E. Koopmans,[3] D. R. Stinebring[5,6] and W. van Straten[4,7,8]

[1] *Manly Astrophysics Workshop Pty Ltd, Unit 3, 22 Cliff Street, Manly, NSW 2005, Australia*
[2] *School of Physics, University of Sydney, NSW 2006, Australia*
[3] *Kapteyn Astronomical Institute, University of Groningen, PO Box 800, 9700 AV Groningen, the Netherlands*
[4] *Netherlands Foundation for Research in Astronomy, PO Box 2, 7990 AA Dwingeloo, the Netherlands*
[5] *Department of Physics and Astronomy, Oberlin College, Oberlin, OH 44074, USA*
[6] *Leiden University Observatory, PO Box 9513, NL-2300 RA Leiden, the Netherlands*
[7] *Center for Gravitational Wave Astronomy, University of Texas, Brownsville, TX 78520, USA*
[8] *Centre for Astrophysics and Supercomputing, Swinburne University of Technology, Hawthorn, VIC 3122, Australia*

ABSTRACT

The dynamic spectrum of a radio pulsar is an in-line digital hologram of the ionized interstellar medium. It has previously been demonstrated that such holograms permit image reconstruction, in the sense that one can determine an approximation to the complex electric field values as a function of Doppler shift and delay, but to date the quality of the reconstructions has been poor. Here we report a substantial improvement in the method which we have achieved by simultaneous optimization of the thousands of coefficients that describe the electric field. For our test spectrum of PSR B0834+06 we find that the model provides an accurate representation of the data over the full 63 dB dynamic range of the observations: residual differences between model and data are noise like. The advent of interstellar holography enables detailed quantitative investigation of the interstellar radio-wave propagation paths for a given pulsar at each epoch of observation. We illustrate this using our test data which show the scattering material to be structured and highly anisotropic. The temporal response of the medium exhibits a scattering tail which extends to beyond 100 μs, and the centroid of the pulse at this frequency and this epoch of observation is delayed by approximately 15 μs as a result of multipath propagation in the interstellar medium.

Key words: scattering – turbulence – techniques: interferometric – pulsars: general – pulsars: individual: B0834+06 – ISM: structure.

Solve for the underlying Electric field!

$$\tilde{E}(\tau, f_d)$$

$$I(t, \nu)$$

$$|\tilde{I}(\tau, f_d)|^2$$

Solve for the underlying Electric field!

$$I(\tau)$$

$$\tilde{E}(\tau, f_d)$$

$$< \tau > (t)$$
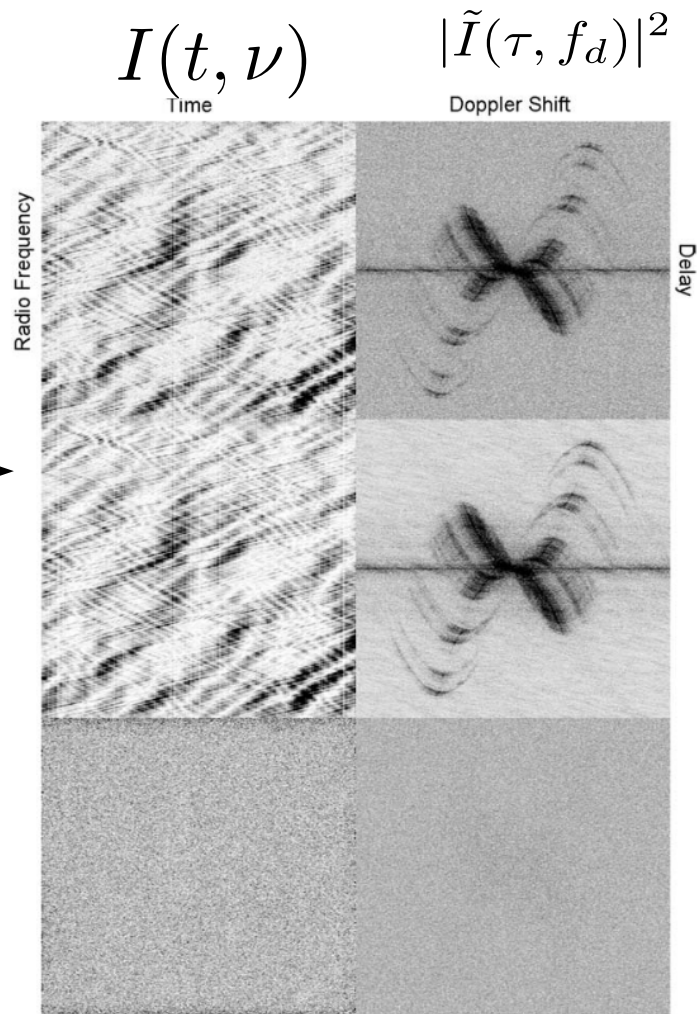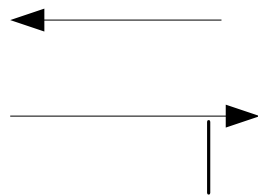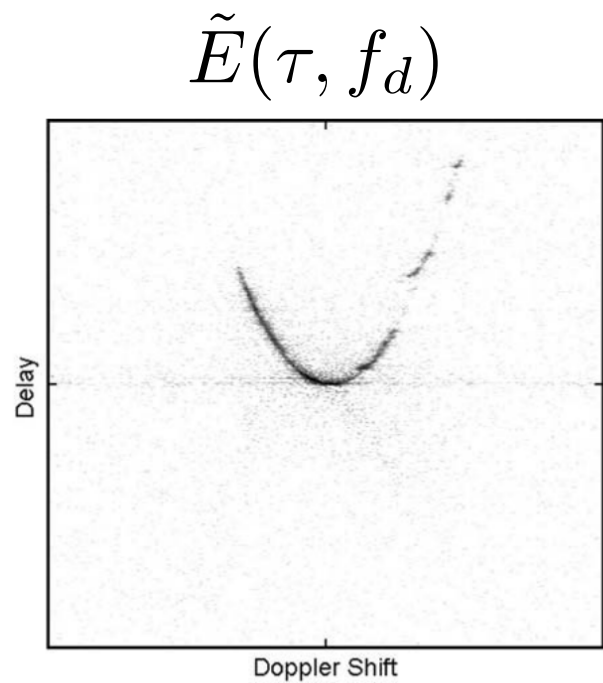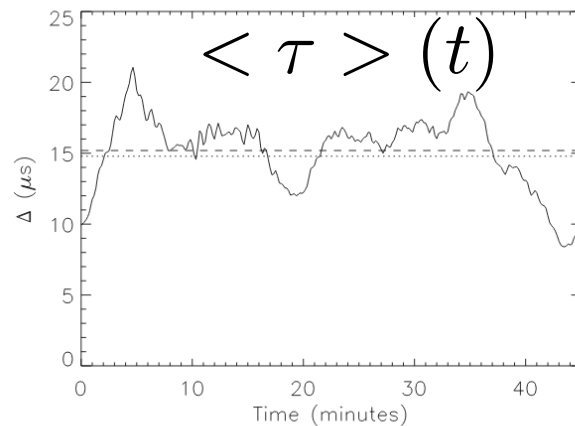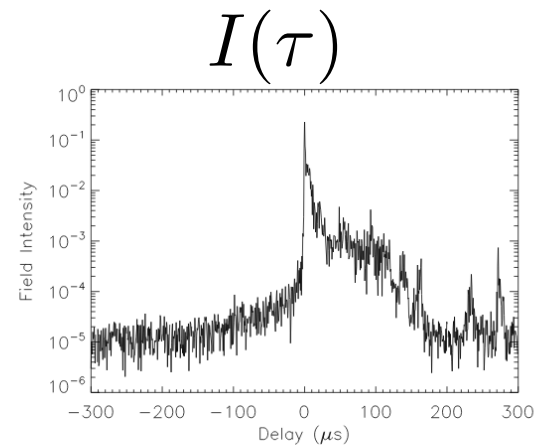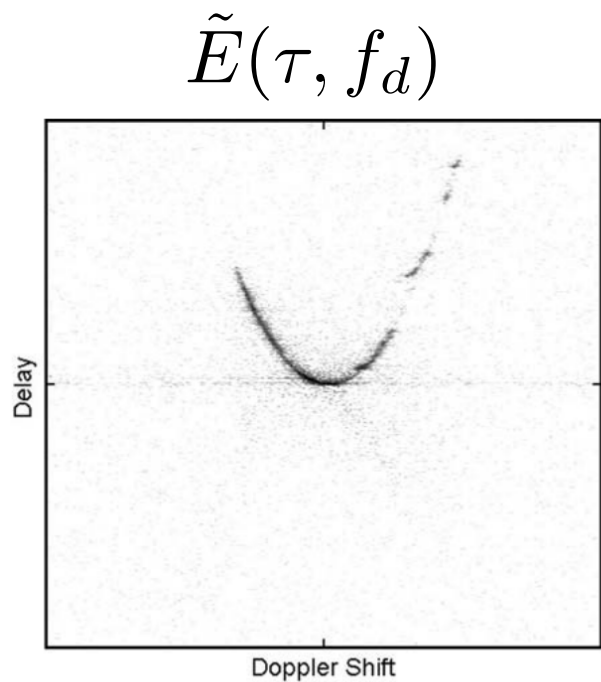
Figure 5. The interstellar propagation delay, $\Delta(t)$ (solid line), as determined from the holographic image shown in Fig. 3 with low amplitude coefficients ($|\tilde{u}_k| < 0.004$) set to zero. Also shown is the (unweighted) mean delay, $\langle \Delta \rangle = 15.2$ µs (dashed line), for the observation. The dotted line shows a weighted mean (14.8 µs), with the weight for each time sample being equal to the intrinsic pulsar flux, f_k, as determined by the modelling procedure described in Section 2 of this paper.

- Time offset between telescopes as diffraction pattern sweeps across the earth

- Detected with VLBI as a phase $\phi = 2\pi \vec{b} \cdot \vec{\theta}/\lambda$

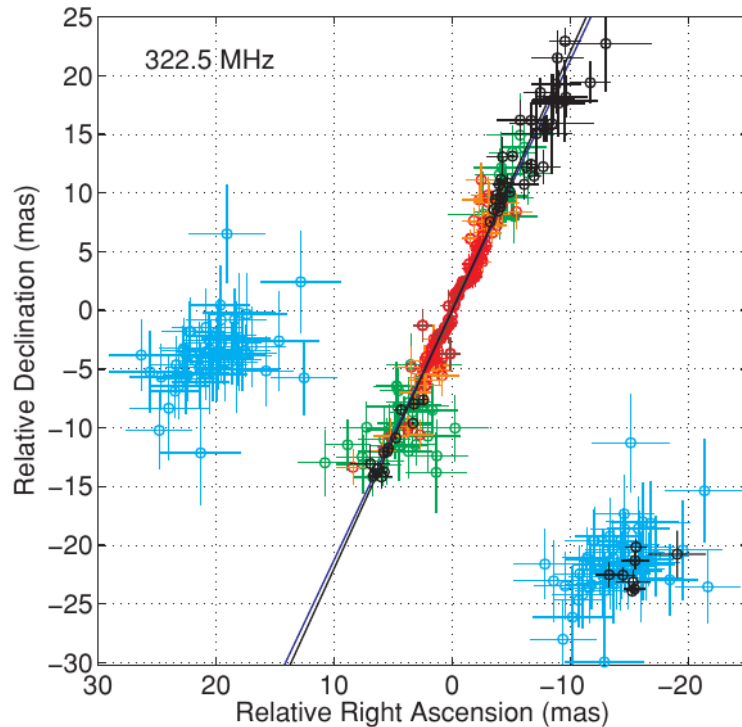Amplitude   Phase
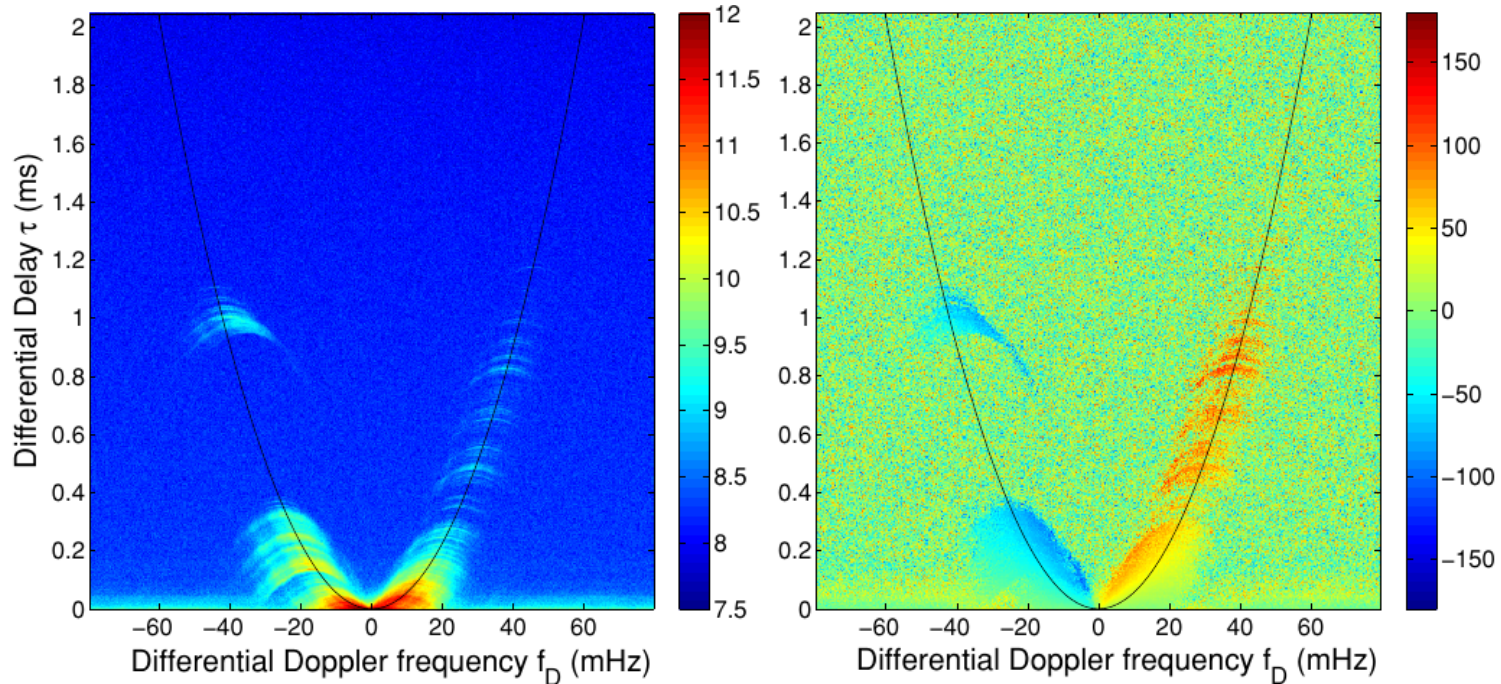
- Time offset between telescopes as diffraction pattern sweeps across the earth

- Detected with VLBI as a phase
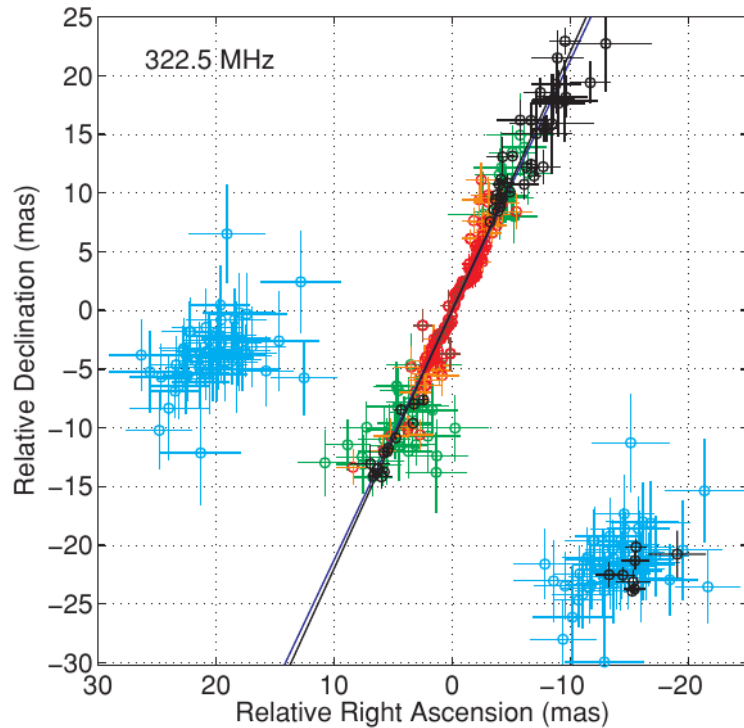
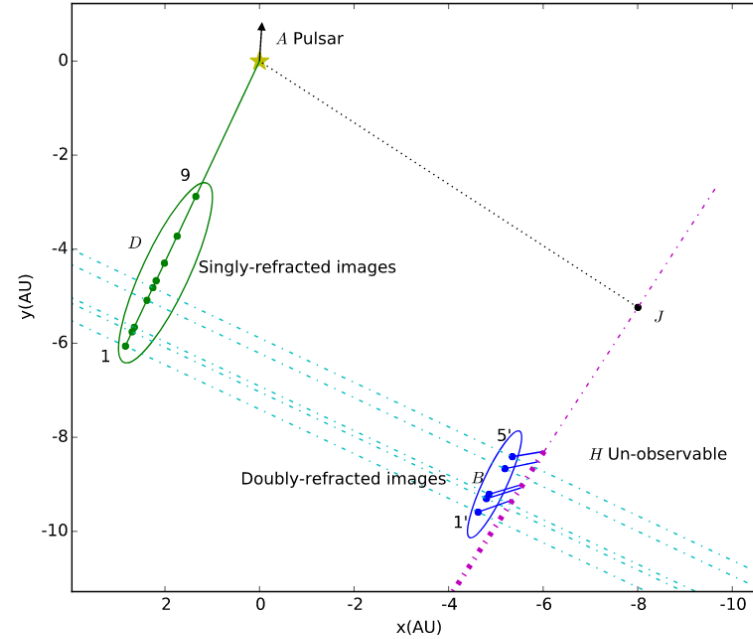- Time offset between telescopes as diffraction pattern sweeps across the earth

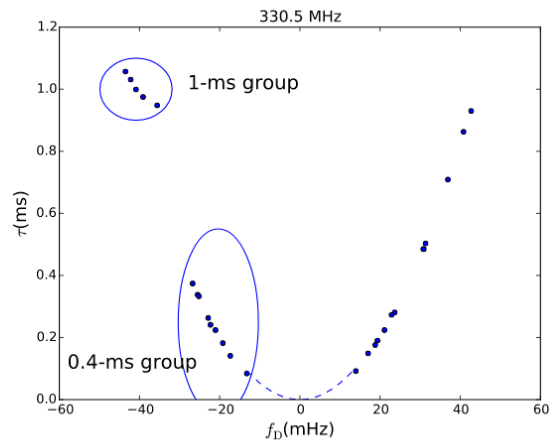- Detected with VLBI as a phase

Analogy – images on a lake surface

Double Refraction? - Siqi Liu et al. 2016

Arclets stable over ~1 month

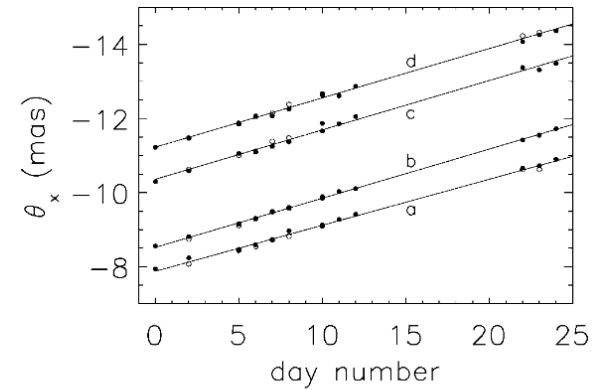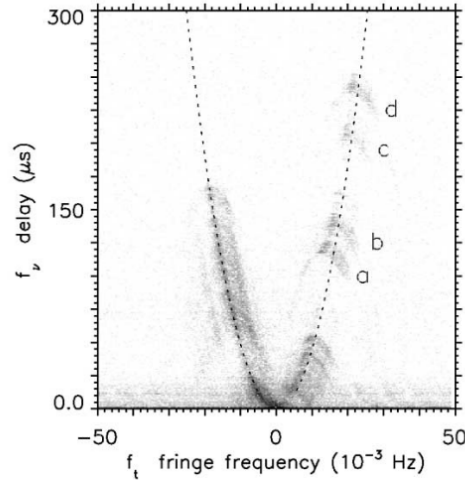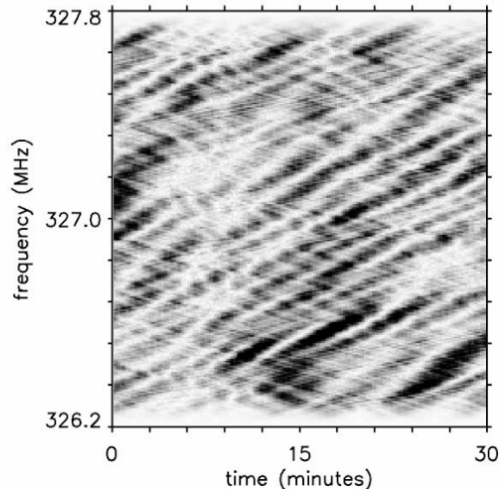Move uniformily, consistent with pulsar's proper motion

FIG. 4.—Angular position of four arclets over 26 days of observations at two observing frequencies (day 0 = 2003 December 31). As in Fig. 3, filled circles denote 321 MHz data, and open circles indicate 334 MHz data. The uniform consistent motion of the arclets is due primarily to the motion of the pulsar, indicating that arclets are caused by scattering objects essentially stationary in the screen.
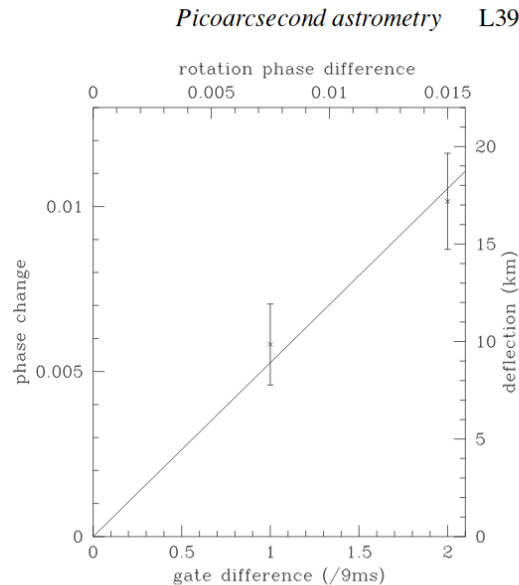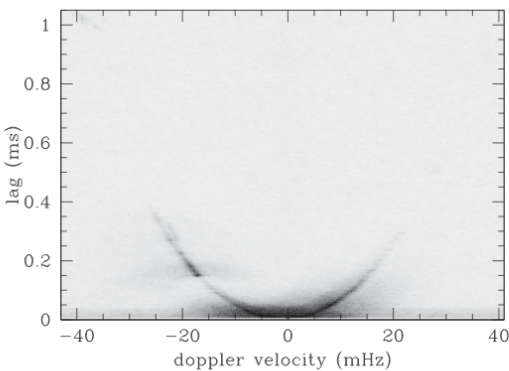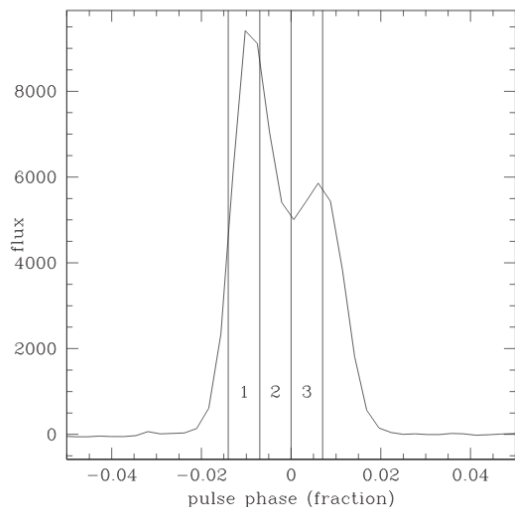
If pulsar moves, scintillation pattern changes slightly

- Compare scintillation across pulse phase, look for positional shifts

- "Interstellar Interferometer"

$$\tilde{E}(\tau, f_d)$$

For each phase bin, correlate...

Figure 6. Pulsar motion projected along scattering axis. The horizontal axis is the time difference and the vertical axis is the apparent motion shift along the scattering axis, scaled to a Doppler frequency of −15mHz. The changes are always small. The error is about 1/1000th of a radian, which reflects the extremely high S/N of the measurement.
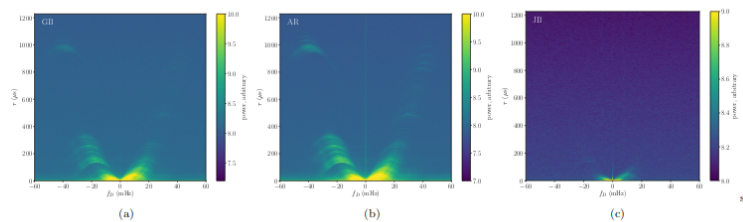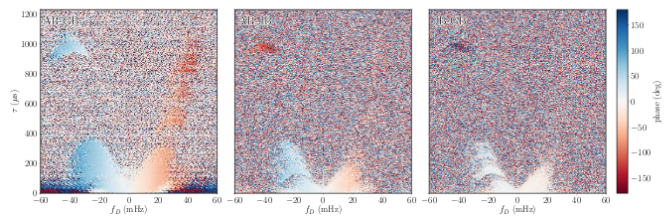
Figure 2. The secondary spectra of PSR B0834+06 as observed from Green Bank (Fig. 2a), Arecibo (Fig. 2b) and Jodrell Bank (Fig. 2c). The colour scale corresponds to the base 10 log of the power (in arbitrary units). Note that the scale varies between stations.
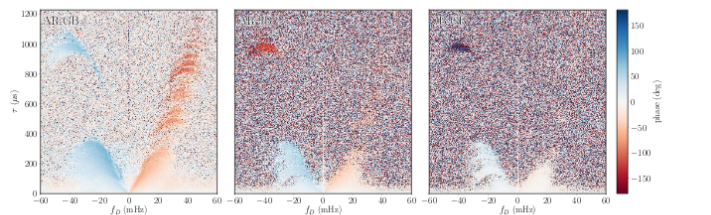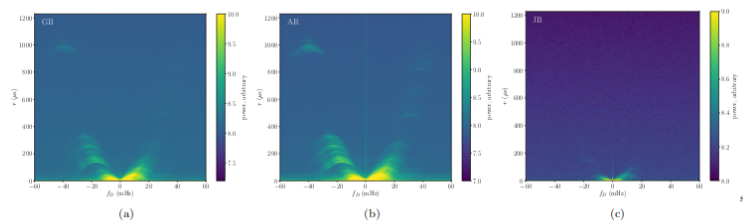

Figure 3. The phases (in radians) of the visibility cross-spectra, $S_V(\tau, f_D)$, for the Green Bank-Arecibo (left), Jodrell Bank-Arecibo (center) and Green Bank-Jodrell Bank (right) baselines. Here, $\phi_{V,jk} = \frac{2\pi}{\lambda}(\boldsymbol{\theta}_j + \boldsymbol{\theta}_k) \cdot \mathbf{b}$, so that along any inverted arclet the phase is large at low $|f_D|$, when the two images interfering are close together on the sky, and small at large $|f_D|$, when the two images interfering are on opposite sides of the pulsar, but roughly the same angular distance from the pulsar. There is a feature at 1 ms that does not follow the phase trend of the main parabolic feature, indicating that it is from a scattering screen with a different orientation, distance, and/or velocity than that responsible for the main parabolic feature, as determined by Brisken et al. (2010). These are the quantities used in the analysis of PSR B0834+06 by Brisken et al. (2010) and the left-most panel is a reproduction of their Fig. 1.
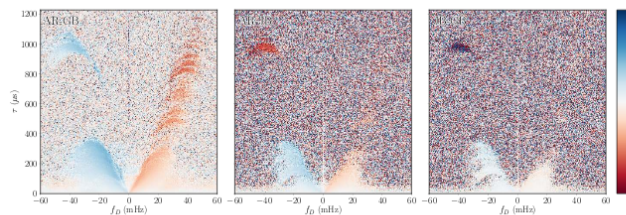

Figure 4. The phases (in radians) of the intensity cross secondary spectra between Green Bank and Arecibo (left), Jodrell Bank and Arecibo (center), and Green Bank and Jodrell Bank (right). Here, we expect a linear gradient in phase with f_D if the scattering is due to a single screen. (See equation (11).) We see that the main parabolic structure does follow a phase gradient, but there is another feature at 1 ms, that does not follow this gradient in the JB-AR and GB-JB spectra. This suggests that it is not from the same scattering screen as the main parabolic arc, consistent with the analysis by Brisken et al. (2010).

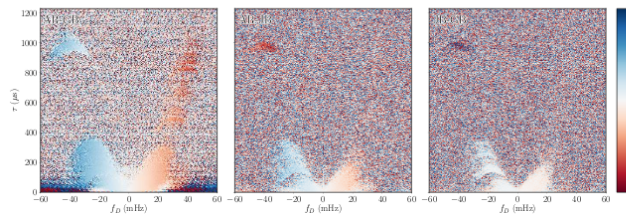$$\tilde{E}_1 \tilde{E}_2 \rightarrow \phi = 2\pi \vec{b} \cdot (\vec{\theta_j} - \vec{\theta_k})/\lambda$$

$$\tilde{I}_1 \tilde{I}_2 \rightarrow \phi = 2\pi \vec{b} \cdot (\vec{\theta_j} + \vec{\theta_k})/\lambda$$
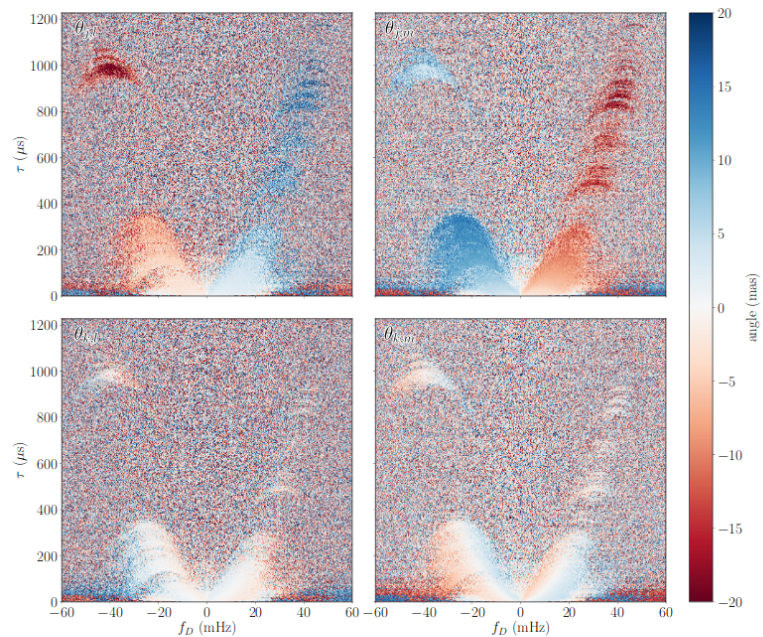
Figure 2. The secondary spectra of PSR B0834+06 as observed from Green Bank (Fig. 2a), Arecibo (Fig. 2b) and Jodrell Bank (Fig. 2c). The colour scale corresponds to the base 10 log of the power (in arbitrary units). Note that the scale varies between stations.
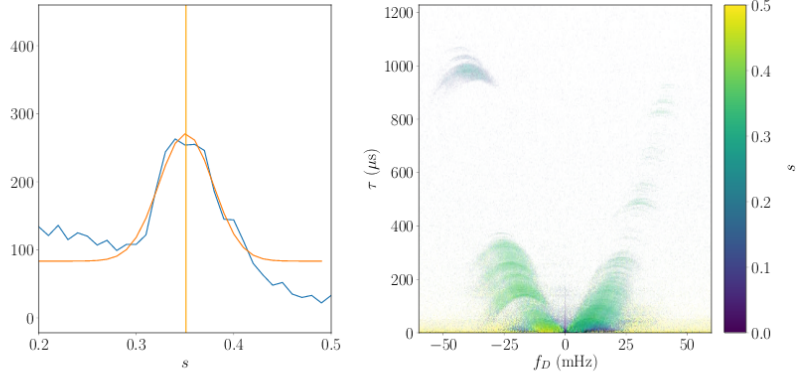

Figure 3. The phases (in radians) of the visibility cross-spectra, $S_V(\tau, f_D)$, for the Green Bank-Arecibo (left), Jodrell Bank-Arecibo (center) and Green Bank-Jodrell Bank (right) baselines. Here, $\phi_{V,jk} = \frac{2\pi}{\lambda}(\boldsymbol{\theta}_j + \boldsymbol{\theta}_k) \cdot \mathbf{b}$, so that along any inverted arclet the phase is large at high $|f_D|$, when the two images interfering are close together on the sky, and small at low $|f_D|$, when the two images interfering are on opposite sides of the pulsar, but roughly the same angular distance from the pulsar. There is a feature at 1 ms that does not follow the phase trend of the main parabolic feature, indicating that it is from a scattering screen with a different orientation, distance, and/or velocity than that responsible for the main parabolic feature, as determined by Brisken et al. (2010). These are the quantities used in the analysis of PSR B0834+06 by Brisken et al. (2010) and the left-most panel is a reproduction of their Fig. 1.


Figure 4. The phases (in radians) of the intensity cross secondary spectra between Green Bank and Arecibo (left), Jodrell Bank and Arecibo (center), and Green Bank and Jodrell Bank (right). Here, we expect a linear gradient in phase with f_D if the scattering is due to a single screen. (See equation (11).) We see that the main parabolic structure does follow a phase gradient, but there is another feature at 1 ms, that does not follow this gradient in the JB-AR and GB-JB spectra. This suggests that it is not from the same scattering screen as the main parabolic arc, consistent with the analysis by Brisken et al. (2010).

Figure 8. The left-hand panel shows the histogram of values of s (measured with the AR-GB/AR-JB baseline pair) for pixels where $\theta_k < 1$ mas. Fitting a Gaussian between $s = 0.2$ and $s = 0.5$, we find $s = 0.35 \pm 0.03$. The right-hand panel shows the value of $s = 1 - \frac{d_{\text{lens}}}{d_{\text{psr}}}$ calculated at each pixel in the secondary spectrum using the AR-GB/AR-JB baseline pair. An alpha-mask that is log-spaced in the absolute power of the visibility secondary cross-spectrum has been applied to allow points of interest to stand out. From this panel, it is obvious that the 1-ms feature is from a different screen than the main parabola.
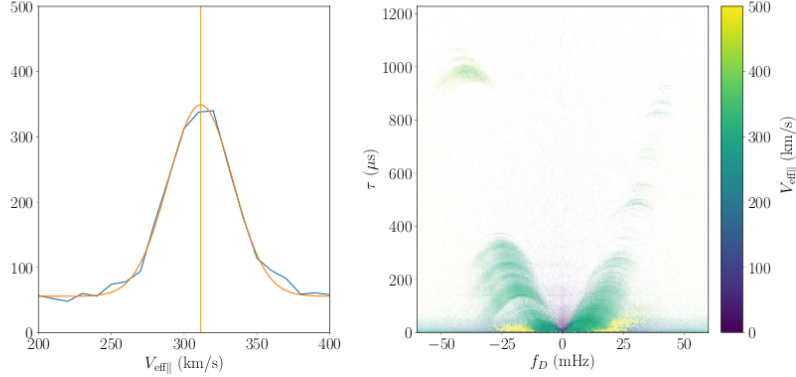
Figure 9. The left-hand panel shows the histogram of values of $V_{\text{eff}\parallel}$ (measured with the AR-GB/AR-JB baseline pair) for pixels where $\theta_k < 1$ mas. Fitting a Gaussian between 200 km/s and 350 km/s, we find $V_{\text{eff}\parallel} = 300 \pm 30$ km/s. The right-hand panel shows the value of $V_{\text{eff}\parallel}$ calculated at each pixel in the secondary spectrum (using the AR-GB/AR-JB) baseline pair). An alpha-mask that is log-spaced in the absolute power of the visibility secondary cross-spectrum has been applied to allow points of interest to stand out.